
MESHGRAPHNET-TRANSFORMER: SCALABLE MESH-BASED LEARNED SIMULATION FOR SOLID MECHANICS

M. M. Iparraguirre, I. Alfaro, D. González, E. Cueto

Keysight-UZ Chair of the National Strategy on Artificial Intelligence,
Aragon Institute of Engineering Research (I3A), Universidad de Zaragoza, Zaragoza, Spain.

{mikel.martinez,iciar,gonzal,ecueto}@unizar.es

ABSTRACT

We present MeshGraphNet-Transformer (MGN-T), a novel architecture that combines the global modeling capabilities of Transformers with the geometric inductive bias of MeshGraphNets, while preserving a mesh-based graph representation. MGN-T overcomes a key limitation of standard MGN, the inefficient long-range information propagation caused by iterative message passing on large, high-resolution meshes. A physics-attention Transformer serves as a global processor, updating all nodal states simultaneously while explicitly retaining node and edge attributes. By directly capturing long-range physical interactions, MGN-T eliminates the need for deep message-passing stacks or hierarchical, coarsened meshes, enabling efficient learning on high-resolution meshes with varying geometries, topologies, and boundary conditions at an industrial scale.

We demonstrate that MGN-T successfully handles industrial-scale meshes for impact dynamics, a setting in which standard MGN fails due message-passing under-reaching. The method accurately models self-contact, plasticity, and multivariate outputs, including internal, phenomenological plastic variables. Moreover, MGN-T outperforms state-of-the-art approaches on classical benchmarks, achieving higher accuracy while maintaining practical efficiency, using only a fraction of the parameters required by competing baselines.

Keywords MeshGraphNets, Under-reaching, Transformers, Physics-Attention, Impact Dynamics, Plasticity

1 Introduction

Traditional solvers in solid mechanics are predominantly based on the finite element method (FEM), which can provide high-fidelity solutions when coupled with accurate physics-based models, but at a high computational cost, especially for many-query problems. Their accuracy depends critically on fine spatial meshes and, in explicit dynamics, small time steps: insufficient spatial resolution may cause an undesirable level of error, while coarse temporal discretization can lead to solutions that deviate from the governing partial differential equations, causing non-compliance with energy conservation laws for purely numerical reasons. Achieving reliable accuracy therefore requires very fine discretizations, significantly increasing computational demands. Human knowledge is embedded in the physical models, which describe point-level behavior through constitutive equations, and in the PDEs and boundary conditions defined by the engineer. Deep learning takes this one step further by enabling models to learn from the results of these simulations, effectively capturing and reusing prior knowledge to accelerate future predictions. While this approach can substantially speed up simulations, it does not yet fully replace FEM, as it still requires high-fidelity data for training and generalizes reliably, in general, only to scenarios similar to those seen during training [5, 6, 27].

This work focuses on learning from high-fidelity simulations by leveraging physics knowledge during training. Graph Neural Networks (GNNs) naturally operate on graph-structured inputs, as are the models obtained using finite elements, where nodes store state variables and edges follow mesh connectivity. Sanchez-Gonzalez *et al.* [17] first applied GNNs to physics simulation in a particle-based setting, while Pfaff *et al.* [18] extended this to Lagrangian meshes with MeshGraphNets (MGN) for quasi-static collisions. Other examples of similar architectures include [2–4, 11, 12], among

others. A version that incorporates thermodynamic inductive biases and improves the accuracy of the method can be found in [7–10, 14, 15]. They all rely on Message Passing Neural Networks (MPNNs), which compute predictions through iterative node-to-node exchanges rather than processing the full graph globally [1]. Each node updates its state by aggregating information from its neighbours, providing a strong local bias that mimics the local character of the equations of Elasticity. However, this locality is also the main limitation: physical phenomena must be within the effective message-passing reach, making the number of message-passing iterations critical for the model’s accuracy; otherwise, it will suffer from under-reaching, as shown by Tesan *et al.* [22]. This node-centric formulation provides strong geometric flexibility, allowing MGN models to generalize to unseen meshes given node features and connectivity. However, long-range interactions are captured only if a sufficient number of message-passing layers is used, which becomes intractable for large meshes and computationally inefficient [13].

Several works have attempted to address these limitations. BSMS-GNN [32] employs a bi-stride pooling strategy based on breadth-first search to construct hierarchical representations without manually designed coarse meshes, using a U-Net-like architecture. Similarly, ROBIN, proposed by Würth *et al.* [21], combines diffusion processes with AMB-based pooling to preserve high-frequency information and node density, demonstrating strong performance on 2D benchmark problems. EvoMesh [35] introduces adaptive graph hierarchies through anisotropic message passing and context-aware hierarchical node selection. More recently, M4GN [37] is a hierarchical graph surrogate that operates on meshes segmented via a hybrid mesh-graph scheme. It requires an explicit preprocessing step to compute the mesh-graph segmentation and modal-decomposition features prior to training and inference. Importantly, all these methods have been evaluated primarily on benchmark datasets rather than industrial-scale simulations. For more industry-like problems, ReGUNet, introduced by Li *et al.* [20], extends MeshGraphNets with a recurrent hierarchical U-Net and was the first to demonstrate crashworthiness simulation on an automotive B-pillar. While its hierarchical design and history handling mitigate error accumulation, the reliance on a fixed coarse mesh limits its ability to generalize to geometries that differ significantly from those seen during training. Overall, hierarchical approaches partially alleviate the limitations of deep message passing, but they do so by introducing coarse representations that are difficult to automate and costly in practice. Moreover, although message-passing under-reaching is reduced at coarser levels, it is not eliminated.

As an alternative to MPNN-based methods, Transformers have proven effective for handling large numbers of nodes, since they process nodes in parallel and can capture global phenomena without iterative message passing. Y. Yu *et al.* [19] introduced HCMT, a mesh-based method that employs a learnable pooling strategy with transformers. However, most of existing Transformer-based approaches are typically meshless, operating only at the node level and ignoring important structural information such as mesh connectivity, self-contact, collisions, or tied constraints, which serve as local biases in physical simulations. Two works are particularly relevant in this context. Transolver [29] introduced a physics-based tokenization that overcomes the limitation of fixed node counts, providing insight into how attention mechanisms capture relationships between regions of a component and the underlying physical structure. Its extension, Transolver++ [28], further improves attention precision through a learnable eidetic slicing technique, enabling sharper modelling of interactions across the component. Both approaches are fully end-to-end and data-driven, learning solely from node features without incorporating any problem-specific boundary conditions. Universal Physics Transformer [30] is a Transformer-based neural operator for volumetric CFD meshes that captures boundary and interior structure via anchor-attended tokens, but has not been applied, to the best of our knowledge, to Lagrangian systems with stress or contact constraints, as in solid mechanics.

The main contributions of this work are:

- **MeshGraphNet-Transformer (MGN-T):** We introduce MGN-T, an extension of the MeshGraphNet architecture that removes the message-passing under-reach bottleneck. The processor combines two MPNN blocks for local updates, pre-processor and refinement, and a Transformer physics-attention for global updates.
- **Efficient global updates while preserving mesh-based structure:** This mesh-based approach that keeps the powerful feature engineering of MGN, which explicitly models collisions and self-contact, while capturing long-range interactions across the mesh in a single global update.
- **Scalability and generalization:** MGN-T generalises to different geometries, mesh topologies, and boundary conditions, and it is capable of simulating highly non-linear phenomena such as plasticity, efficiently scaling to high-resolution industrial simulations.

The outline of the paper is as follows. In Section 2, we present the basic ingredients of the method. In Section 3 we introduce the different benchmarks employed to show the capabilities of the just developed method. These are thoroughly analyzed in Section 4, where they are compared to state-of-the-art methodologies. The paper is finished with a brief discussion in Section 5.

2 Methodology

We focus on developing a neural PDE solver for solid mechanics trained on synthetic data coming from high-fidelity simulations. The solver must handle high-resolution meshes in which the number of nodes, geometries, and boundary conditions may vary and, additionally, collision interactions and self-contact on highly non-linear materials, including elasto-plastic behaviour.

We analyze first a problem of impact dynamics using the pi-beam benchmark, provided by ESI Group, Keysight Technologies, as a real-world engineering application and also a quasi-static regime example using the deforming plate dataset, defined in [17].

2.1 Feature engineering

Each component or part in the physical system is represented as a graph $G(V, E_M)$, where nodes correspond to mesh vertices V and mesh edges E_M encode connectivity. In contact or collision scenarios, the system is modeled as a multi-graph, where initially disjoint component graphs are dynamically connected through contact edges E_C when contact occurs. For multi-component bodies, tied constraints are encoded as mesh edges computed using a k -nearest neighbour procedure over the assembled components, remaining fixed during simulation.

Physical variables may differ across problems, emphasizing the importance of selecting the nodal variables that encode the initial and boundary conditions of the problem, as these determine the final physical state.

Node features: Each node i has a state vector s_i containing problem-specific physical variables or parameters (e.g., velocity or shell thickness), and a one-hot encoded vector which indicates the node type n_i (e.g., deformable component or rigid body). The node feature vector is defined as $v_i = (s_i, n_i)$.

Edge features: We encode geometric information using relative positional variables to maintain spatial equivariance. We consider two types of edges:

- Mesh edges: $e_{ij}^M \in E_M$ defined by mesh connectivity and tied constraints which represent local interactions. For each edge (i, j) , we encode relative distances between connected nodes in the reference and current configurations:

$$e_{ij}^M = (\mathbf{X}_i - \mathbf{X}_j, \|\mathbf{X}_i - \mathbf{X}_j\|, \mathbf{x}_i^t - \mathbf{x}_j^t, \|\mathbf{x}_i^t - \mathbf{x}_j^t\|).$$

- Contact edges: $e_{ij}^C \in E_C$ defined by nodes within a contact radius r_c , if $\|e_{ij}^C\| < r_c$. This includes both ground-component contact and self-contact. For each contact edge, we encode the relative distance between connected nodes in the current configuration:

$$e_{ij}^C = (\mathbf{x}_i^t - \mathbf{x}_j^t, \|\mathbf{x}_i^t - \mathbf{x}_j^t\|).$$

Positional encoding: We construct a stationary-wave representation over the component’s spatial domain in the undeformed configuration to avoid reliance on absolute positions. Specifically, sinusoidal functions are defined along the length, width, and height of the component [16].

2.2 Architecture

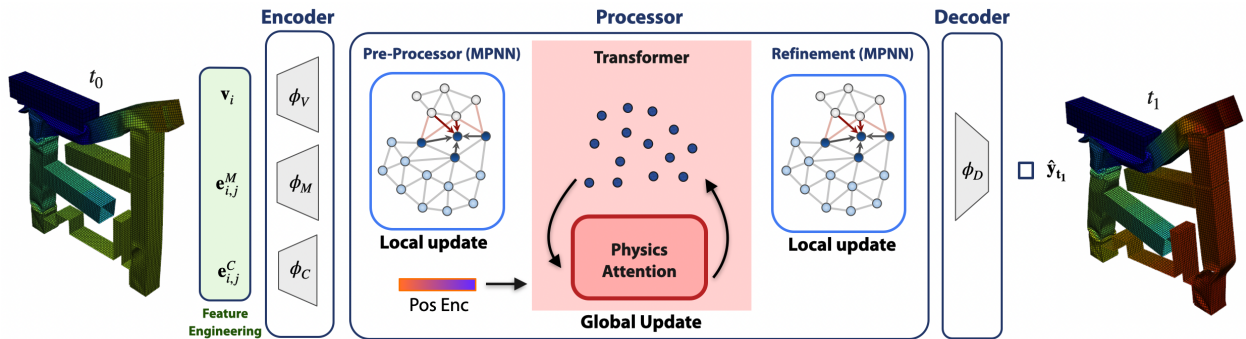


Figure 1: Illustration of the MGN-T architecture. Processor: Pre-processor MPNN (local update), Transformer processor with physics-attention (global update) and Refinement processor MPNN (local update).

The proposed MeshGraphNet-Transformer (MGN-T) architecture follows the Encoder–Processor–Decoder scheme illustrated in Figure 1. The model is trained using 1-step predictions and then at inference integrates them for long rollouts following an autoregressive approach. Unlike standard MeshGraphNets, where the processor consists of a deep stack of message-passing layers, MGN-T replaces this iterative structure with a Transformer as a global processor that captures long-range interactions across the mesh.

Encoders: Three dedicated encoders map the node and edge features into a high-dimensional latent space :

$$\varepsilon_i^V = \phi_V(\mathbf{v}_i), \quad \varepsilon_{ij}^M = \phi_M(\mathbf{e}_{ij}^M), \quad \varepsilon_{ij}^C = \phi_C(\mathbf{e}_{ij}^C).$$

Processor: The processor consists of three stages: a pre-processing MPNN, a Transformer as the global processor, and a refinement MPNN. The pre-processing and refinement stages are implemented as MPNN blocks and are responsible for local message passing between nodes and edges.

The pre-processing MPNN performs two message-passing iterations to absorb boundary conditions and local interactions. In particular, it allows connected nodes to gather information from neighbors at a 2-hop graph distance before the global update takes place. This step is essential, as MPNNs are the only component of the architecture that explicitly leverage edge information and enforce mesh-based locality, due to message passing.

The Transformer processor performs the global update of node features using two stacked Transformer blocks with physics-attention, see Section 2.3. Before being fed into the Transformer, node attributes are concatenated with positional encodings and projected to match the multi-head attention dimensions. The slicing mechanism of the physics-attention projects the N nodes into P latent physical tokens. By operating on these tokens, the Transformer enables efficient information exchange across these. Then, the de-slicing mechanism projects P back onto N mesh nodes, efficiently completing the global update of the mesh.

Finally, the refinement MPNN performs two message-passing iterations, reinforcing geometric inductive biases and local consistency by updating node and edge features and refining the latent features for decoding.

Decoder: Projects the updated latent node features ε_i^V to the physical space, estimating the variables of interest. $\hat{\mathbf{y}}_i = \phi_D(\varepsilon_i^V)$.

All above ϕ are a 2-layer MLP with LeakyReLU activations, and layer normalization.

2.3 Physics-attention with eidetic states

We adopt the physics-attention mechanism introduced in Transolver [29] and its extension with eidetic states proposed in Transolver++ [28]. Their proposed physics-attention reduces the quadratic complexity $\mathcal{O}(N^2)$ of standard self-attention by projecting N node features into P physical tokens, as z eidetic states. This projection not only reduces computational cost but also allows easy handling of varying input sizes and efficient scaling to a large mesh, as the complexity now is $\mathcal{O}(P^2)$, with $P \ll N$.

To generate the projection, first, a local adaptive temperature mechanism dynamically adjusts the sharpness of the slice weight \mathbf{w} between each node and the corresponding physical token. Here, the temperature τ is learnt from the node features, $\tau = \{\tau_i\}_{i=1}^N = \{\tau_0 + \text{Linear}(x_i)\}_{i=1}^N$, to increase expressivity to learn relationships between nodes and physical tokens,

$$\{\mathbf{z}_j\}_{j=1}^P = \left\{ \frac{\sum_{i=1}^N w_{ij} \mathbf{x}_i}{\sum_{i=1}^N w_{ij}} \right\}_{j=1}^P,$$

where

$$\mathbf{w} = \text{Softmax} \left(\frac{\text{Linear}(\mathbf{x}) - \log(-\log(\epsilon))}{\tau} \right).$$

Second, the slice reparameterization mechanism with the Gumbel–Softmax trick [31] used to calculate the weights \mathbf{w} . This enables differentiable sampling from the categorical distribution over physical states \mathbf{z} , where the Gumbel noise is a function of $\epsilon \sim \mathcal{N}(0, 1)$. These two techniques, proposed in [28], enable sharper weighting and prevent tokens from collapsing, providing a better latent representation of the physical token states.

Physics-attention is defined as a multi-head attention mechanism [16] over the P physical tokens, where P is a hyperparameter. Each token is linearly projected into Query (Q), Key (K), and Value (V), with dimensionality c . The scaled dot product between the Q and the K produces the attention weights, which are normalised with a Softmax

function. Afterwards, the attention weights are projected onto the V to generate the updated z' physical P tokens,

$$Q, K, V = \text{Linear}(z), \quad z' = \text{Softmax}\left(\frac{QK^T}{\sqrt{c}}\right)V.$$

2.4 Model training

MGN-T is trained using teacher-forced on 1-step predictions. Let N be the number of nodes per trajectory and B the batch size, representing snapshots from the same trajectory. The ground truth node outputs are denoted as \mathbf{y}_i^b and the model predictions as $\hat{\mathbf{y}}_i^b$, where $i = 1, \dots, N$ and $b = 1, \dots, B$. It is important that batch samples belong to the same trajectory to ensure consistent matrix reshaping before applying the Transformer processor; this only affects for batch training. The training loss is defined as the mean squared error (L_2 loss), computed per node and averaged over the batch across deformable body nodes:

$$\mathcal{L} = \frac{1}{B} \sum_{b=1}^B \frac{1}{N} \sum_{i=1}^N \left\| \mathbf{y}_i^b - \hat{\mathbf{y}}_i^b \right\|_2^2. \quad (1)$$

3 Numerical Examples

We consider Lagrangian mesh-based models undergoing large deformations in two distinct regimes: a dynamic impact scenario (Pi-beam benchmark) and a quasi-static scenario problem coined as *Deforming plate*, a widely used public benchmark introduced by Pfaff *et al.* [18] for evaluating surrogate models in solid mechanics. An overview of both datasets is provided in Table 1. The Pi-beam dataset is described in detail in Section 3.1 and Deforming plate dataset in Section 3.2.

3.1 Pi-beam benchmark

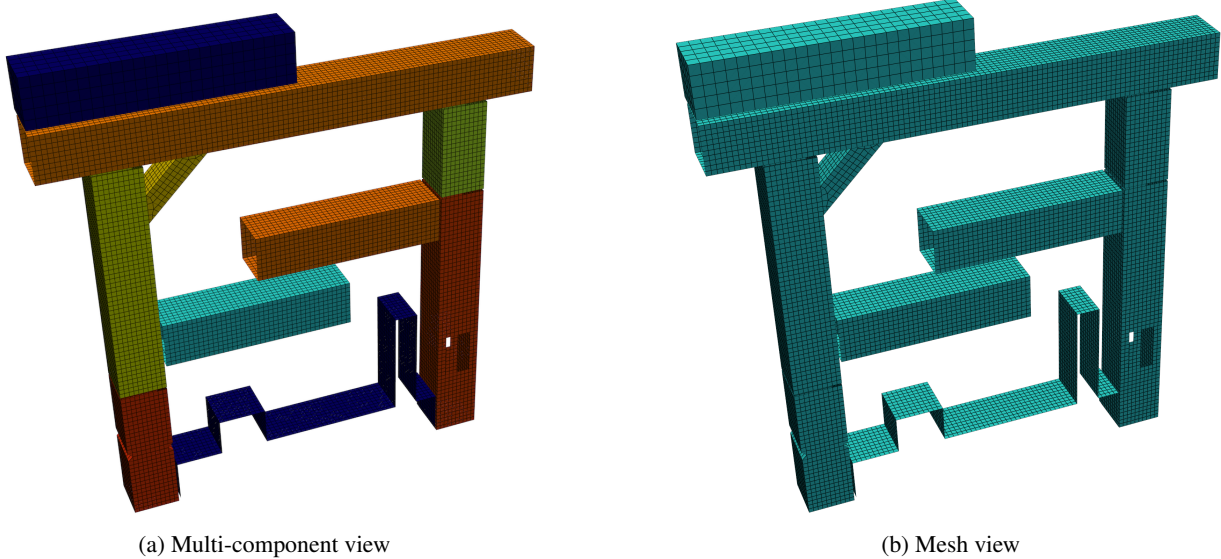


Figure 2: Pi-beam example. (a) Visualization of the multi-component structure, where each colour represents a different component with different thickness. (b) Visualization of the FEM mesh with rectangular shell elements.

The pi-beam benchmark reproduces the impact of a deformable, elastic-plastic, multi-component energy absorber against a rigid obstacle, representing a realistic automotive crash scenario. Three materials are considered: two deformable materials with different stiffnesses and one rigid material. The multi-component structure consists of 9 different tied components with different thickness as described in Figure 2. Each simulation corresponds to a trajectory with varying component thicknesses $k \in (0.1, 0.3)$.

The geometry is discretized using shell elements and a total 16,193 nodes per simulation, where 15,641 belong to the deformable structure and 552 to the rigid obstacle, see Figure 2b. The learning task consists of predicting the full nonlinear dynamic response of the system, including contact, collisions, and subsequent spring-back. Node state

Dataset	Steps	Nodes	Mesh	\mathbf{s}_i	\mathbf{y}_i
Pi-beam	100	16,193	Rect.	$\mathbf{v}_i^t, \alpha_i^t, k_i, \mathbf{n}_i$	$\mathbf{u}_i^{t+1}, \mathbf{v}_i^{t+1}, \alpha_i^{t+1}$
Def. Plate	400	1,250	Teth.	$\mathbf{u}_i^{\text{imp}}, \mathbf{n}_i$	$\mathbf{u}_i^{k+1}, \sigma_{\text{VM},i}^{k+1}$

Table 1: Dataset characteristics and prediction targets.

variables \mathbf{s}_i include thickness k_i , positions \mathbf{x}_i , velocity \mathbf{v}_i , and the plastic hardening variable α_i , which captures the evolving material properties during loading cases (see Table 1). The type of node (rigid, deformable, clamped, ...) is also stored as a one-hot encoder vector \mathbf{n}_i . From each simulation we pruned 100 snapshots, corresponding to a total physical time of 15 ms, or 1.5 ms per considered step.

The dataset is generated using the Pam Crash software (ESI Group, Keysight Technologies), which employs an explicit finite element method (FEM) solver with a temporal resolution of 6.3×10^{-4} ms. The material is assumed to be steel, elastoplastic, with power-law hardening and Young’s modulus $E = 210000$ MPa. One single FE simulation took roughly ten minutes employing four processors and mass scaling. The resulting dataset consists of 28 trajectories in total: 18 for training and validation, and 10 for testing.

3.2 Deforming plate benchmark

While the pi-beam example is intended to check the robustness of the proposed method in the face of changes in the simulation parameter values (in this case, the thicknesses of the different components of the structure), the deforming plate example aims to investigate robustness in the face of changes in the geometry, boundary conditions, and mesh, see [17].

This dataset consists of simulations of an actuator impacting a hyperelastic, deforming plate, in a quasi-static regime. Synthetic data were obtained by employing COMSOL Multiphysics 6.0 (COMSOL, Inc.) The geometries vary, as each simulation has a different distribution of holes in number, radius, and location, as well as the plate thickness. Boundary conditions vary as the clamped sides change and the actuator’s impact location and also prescribed displacements vary. For details, see Table 1.

4 Experiments

We evaluate the model’s performance by means of the root mean squared error on 1-step predictions (RMSE-1) and the full-trajectory (RMSE-all). In addition, we report physical consistency metrics and qualitative visualizations to further analyze the simulated dynamics.

RMSE is computed as the root-mean-square error between predictions and FEM solutions, taken as ground truth, per variable. For each error, we calculate the mean squared error across all feature variables, nodes, time steps, and trajectories, then take the square root (Described in [18], Appendix A.5.2). RMSE-1 is computed without autoregressive rollout: predictions always start from the ground-truth state to prevent error accumulation. Relative RMSE (R-RMSE) follows the same computation, with each error normalized by the infinity norm of the corresponding trajectory (i.e., its maximum magnitude). From now on RMSE and RMSE-all are equivalent.

4.1 Pi-beam

Model	MPNN	Heads	Tokens (P)	Hidden	#Params
MGN	15	–	–	128	2.0M
MGN-T	2 + 2	4	128	64–32–64	0.5M

Table 2: Architectural comparison between baseline MGN and MGN-T.

On the pi-beam dataset, a standard MGN would require more than 175 message-passing iterations to cover the entire component. This lower bound is dictated by the criterion established in [22]. Using fewer iterations leads to *under-reaching*, preventing the network from capturing the relevant physics and resulting in inaccurate predictions. Consequently, this architecture becomes intractable for this example, and even if made tractable, it would be slow due to the large number of required iterations. This scenario is common in industrial-scale simulations like this one.

Model	RMSE			R-RMSE		
	q (mm)	v (mm/ms)	$\alpha \times 10^{-2}$ (mm/mm)	q (%)	v (%)	α (%)
MGN [18]	86.73±0.53	4.55±0.02	2.36±0.013	6.91±0.04	14.81±0.24	7.02±0.17
MGN-T (ours)	8.65±0.79	0.53±0.02	0.65±0.04	0.69±0.06	1.73±0.071	1.94±0.12

Table 3: RMSE and relative RMSE (R-RMSE) comparison between MGN and MGN-T. The interval represents the Standard Error among test trajectories

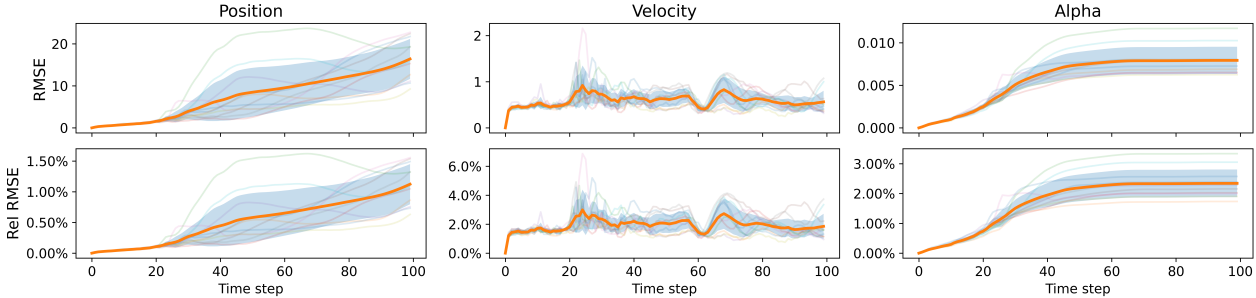


Figure 3: Error evolution rollout comparison between FEM ground truth and MGN-T predictions for the pi-beam benchmark. Line represents the mean and shade the standard error across trajectories. Top: RMSE. Bottom: R-RMSE.

Nevertheless, we include MGN as a baseline using its original configuration of 15-layer MPNNs proposed in [18]. Details about this architecture can be found at Table 2.

Table 3 reports a comparison of absolute and relative errors. As expected, MGN-T outperforms MGN across all variables and metrics, as MGN suffers from under-reach due to insufficient message-passing iterations. In contrast, MGN-T successfully overcomes this limitation, maintaining the relative errors way below 5%, as shown in Figure 3.

Figure 4a illustrates the prediction of a full trajectory and how the nodes that undergo plasticity evolve, highlighting that these are highly localized. Figure 4b shows the velocity magnitude at each time step for consecutive predictions, starting from the beginning of the trajectory. MGN-T accurately predicts buckling, particularly high on the top left side of the component, at a temporal resolution where FEM cannot operate, demonstrating its outstanding capability to handle large temporal steps.

Plasticity evolution and physical consistency: We evaluate physical consistency by analyzing the evolution of the plastic hardening variable α , which, according to yield criteria, should increase monotonically. As a proxy for measuring the level of plastification, we visualise the sum of hardening across nodes at each temporal increment. Similarly, for the velocity we calculate the kinetic energy. Figure 5 compares the predicted and ground-truth plastic hardening and system kinetic energy over time. MGN-T closely follows the FEM solution, preserving monotonic hardening throughout the simulation, in agreement with plasticity theory. The same consistency is observed for the kinetic energy, which decreases as the system dissipates energy during plastification and gathers potential elastic energy, then recovered as kinetic energy during springback. These results indicate that MGN-T respects key physical constraints of plasticity and the corresponding relationships with other state variables.

Physics-attention visualization and interpretability: While directly interpreting the learned token representations remains challenging, visualizing the slice weights w provides valuable qualitative insight into what the model has learnt under the hood (see Figure 6). The weights w illustrate how information from the full mesh is aggregated into each P token. From our perspective, these physics tokens can be interpreted as a *dynamic hierarchical representation* of the system. Unlike classical hierarchical GNNs, where the coarse-to-fine mapping is fixed by a predefined mesh coarsening strategy and determined solely by the spatial domain, the tokenization in MGN-T is learned and adapts based on the current latent nodal states and their encoded spatial context. This allows the model to construct an implicit hierarchy that evolves throughout the simulation, responding to changes in state variables and geometry. The weights concentrate on physically relevant regions, such as highly deformed and plastified regions (see Figure 6a), impact surfaces (see Figure 6d), or broader regions, such as the lower part of the component (see Figure 6c).

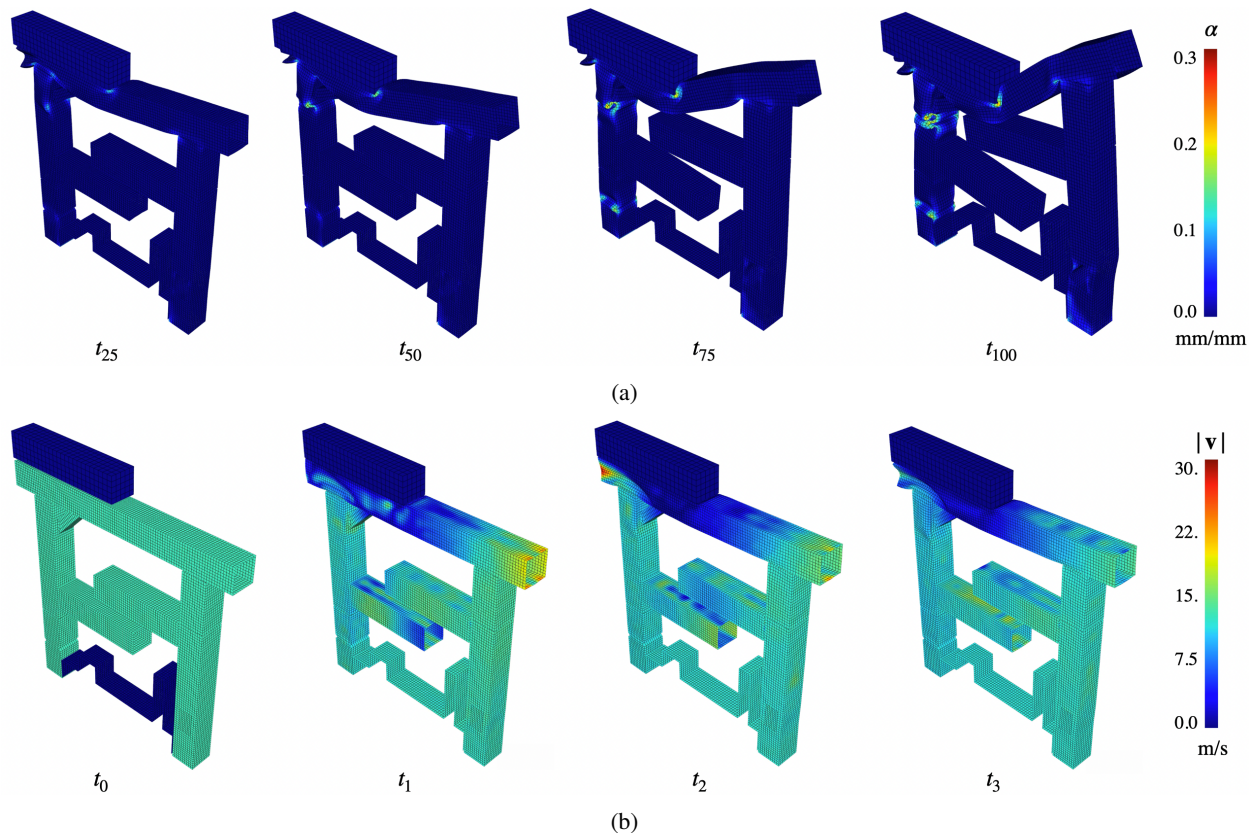


Figure 4: Prediction MGN-T Pi-Beam dataset: MGN-T prediction for a dynamic impact against an obstacle. a) Temporal evolution of hardening variable α . b) Temporal evolution of velocity magnitude $\|v\|$ for consecutive temporal predictions.

Model	RMSE-1	RMSE-all	#Param.	MPNN	Trans.	Hierarchy-free	Coarsen-free
MGN [18]	0.25	15.1	2.0M	✓	×	✓	✓
BSMS-GNN [32]	0.29	16.0	2.8M	✓	×	×	Prior
EvoMesh [35]	0.28	12.9	3.2M	✓	×	×	Learnt
HCMT [23]	–	7.3	2.5M	×	✓	×	Learnt
M4GN [37]	0.26	2.6	2.0M*	✓	✓	×	Prior
MGN-T (ours)	0.10	<u>3.2</u>	0.5M	✓	✓	✓	✓

Table 4: Performance and architectural comparison of baseline models on the Deforming Plate dataset. Left: RMSE errors reported in 10^{-3} . MPNN stands for Message Passing Neural Network, and if employed, Transformers indicates whether the model employs Transformer layers at any point in the architecture; Hierarchy-free specifies whether hierarchical representations are required; and Coarsen-free indicates whether mesh coarsening is required, and if so, its type. Values with * are estimated following the original architecture description, as these were not provided in the original paper.

4.2 Deforming plate

For completeness, we additionally report a comparison table of state-of-the-art baselines benchmarked on the dataset. All the compared baselines are mesh-based methods. In this table, we present the single-step and rollout errors (RMSE-1 and RMSE-All, respectively), together with the total number of trainable parameters for each model (Table 4). This allows for a direct overview of the reported performance–complexity trade-offs across methods. For qualitative visualization of the results, see Figure 7.

Our proposed method achieves competitive performance with state-of-the-art approaches, ranking second in accuracy (but note that it provides a relative error value that is judged sufficient for the vast majority of applications, on the order of 0.6%; see Table 5). Importantly, this result is obtained using only a fraction of the parameters required by other

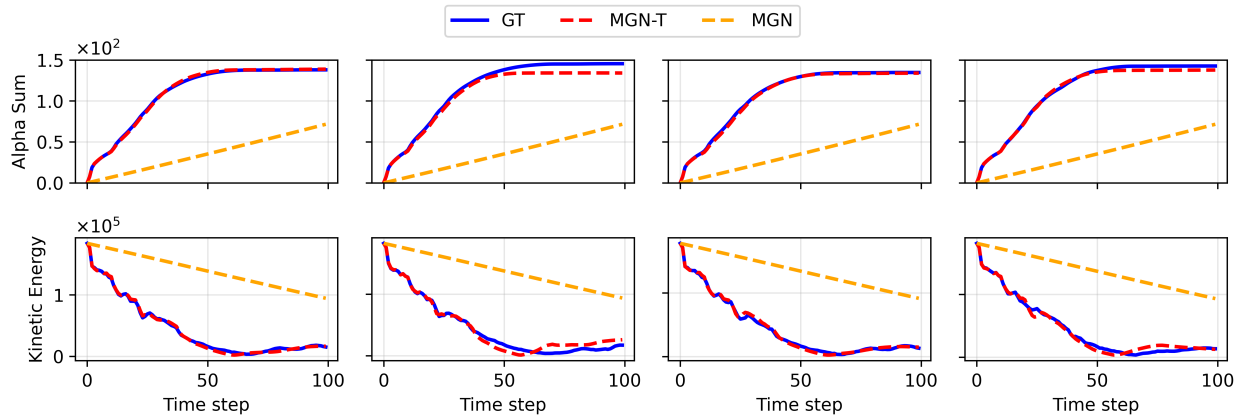


Figure 5: Physical consistency of the pi-beam predictions. Top: Accumulated plastic hardening. Bottom: Kinetic Energy magnitude. Each column represents a different test trajectory, for ground truth, MGN-T and MGN.

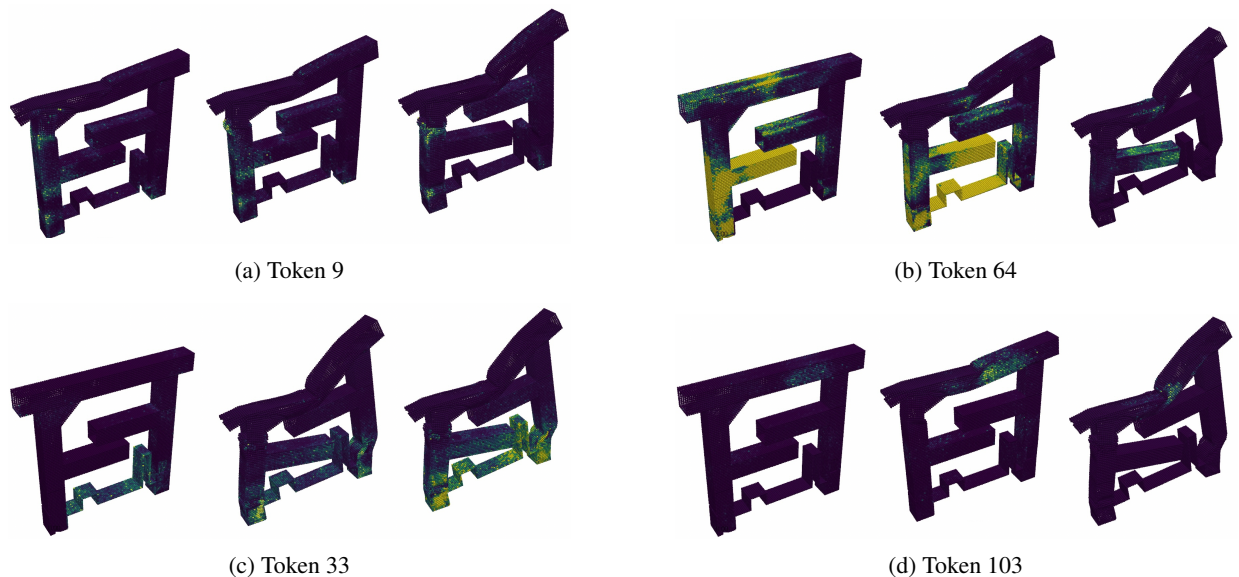


Figure 6: Physics-attention maps for the pi-beam benchmark. Node represents the attention weight corresponding to tokens. Each group has three different snapshots to visualise the evolution of the weights during rollout.

methods. The proposed MGN-T is the only non-hierarchical and coarsening-free method that achieves this level of performance. The Transformer provides an efficient way to perform a global update to prevent under-reaching, which is the main reason for failure of MGN.

HCMT is the only method from the baseline that does not rely on MPNNs but instead uses mesh transformer blocks. Here, stacked blocks of Hierarchical Mesh Transformers (HMT), followed by pooling layers, coarsens the graph. Hierarchical approaches, such as BSMS-GNN construct a hierarchical graph by bi-stride pooling, which groups nodes every other topological depth. The coarse levels are computed prior to training and are non-adaptive. This depth is estimated from the geodetic distance of the mesh using Breadth-First-Search (BFS) from a selected node. This technique is an extension of bipartitioning, which guarantees 2-CC for Directed Acyclic Graphs (DAGs), but, while well-suited to DAGs, might fail to provide the appropriate hierarchy for sophisticated meshes. Here, downsampling and upsampling layers, which connect different coarsening levels, are non-parametric weighted aggregations. On the other hand, EvoMesh relies on differentiable multi-scale graph construction, which has a learnable probability distribution over whether to retain or discard a node at the next coarser graph level. When constructing the multi-level connectivity, the edges of the original mesh are used. Additionally, it incorporates k -hop edges to ensure no disconnected graph partitions, which would limit the message-passing information flow. For communication across coarser levels, reduced and expand layers are learned using the weights estimated by their proposed anisotropic message passing layers. This

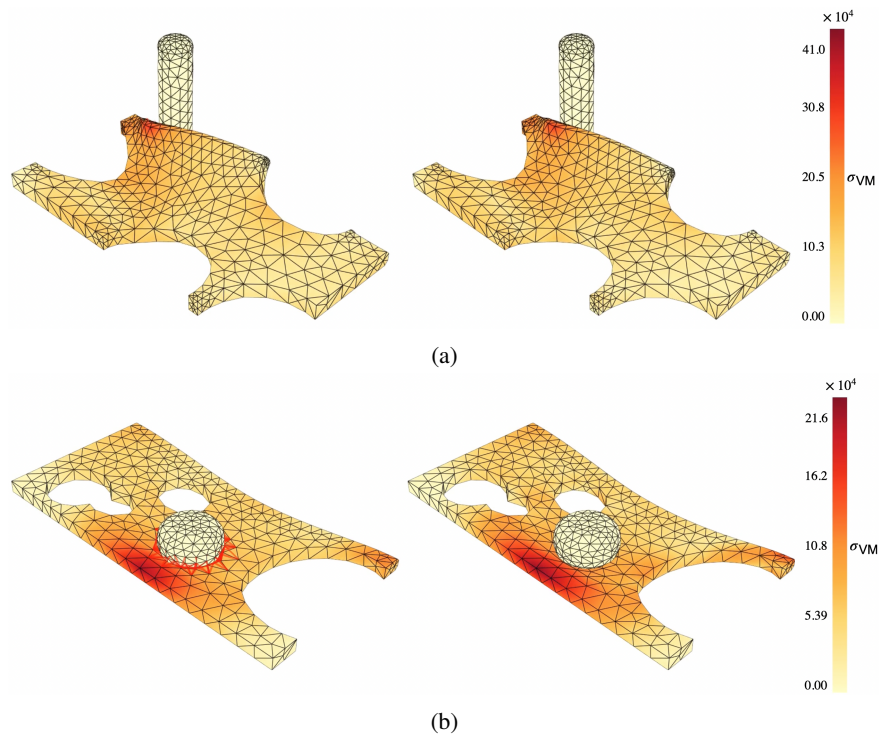


Figure 7: Von Mises stress contour plots for the deforming plate benchmark. Each subplot shows a different test trajectory at step 350, the maximum loading point just before unloading. Left column: MGN-T prediction; right: ground truth. Red edges indicate contacts between the actuator and the plate, determined using a distance criterion.

	RMSE		R-RMSE	
	\mathbf{q} ($\times 10^{-3}$)	σ_{VM} ($\times 10^3$)	\mathbf{q} (%)	σ_{VM} (%)
All-steps	3.16 ± 0.25	5.83 ± 0.34	0.63 ± 0.05	3.61 ± 0.21
1-step	0.10 ± 0.005	3.87 ± 0.17	0.02 ± 0.001	2.5 ± 0.13

Table 5: Performance of the MGN-T model on the Deforming Plate dataset. RMSE and relative RMSE for \mathbf{q} and σ_{VM} , reported for multi-step and 1-step predictions.

method provides a learnable hierarchy construction and coarsening that adapt to latent nodal states, at the cost of increasing the model’s trainable parameters. Nevertheless, despite learnable coarsening being an advantage, it seems like the heuristics employed might have limited the performance of these methods.

M4GN remains the best-performing method, also combining MPNN with Transformers to handle long-range relationships. However, this method does not rely on coarser meshes, rather, segments are calculated prior to training. For the segmentation, they employ a 2-step hybrid segmentation strategy that combines graph partitioning with a superpixel-style refinement step, which is guided by modal decomposition features for physical consistency. Despite their promising results, our method can be trained end-to-end without the need for hierarchy or coarsening, which in many cases is highly domain and geometry-dependent and might not be straightforward.

As mentioned above, MGN-T is the lightest and best-performing method that does not require hierarchy or coarsening. It can be trained end-to-end, offering a more straightforward training pipeline while demonstrating strong off-the-shelf performance.

4.3 Computational Cost

All experiments were executed on a single NVIDIA RTX 4090 GPU (24 Gb) of memory. Inference time consumption is described in Table 6, where t_{model} represents the time consumption of one forward pass and t_{full} includes the preprocessing for each time step. Highlight that, for the pi-beam dataset, MGN suffers from under-reaching. Training

Dataset & Model	t_{model} (ms/step)	t_{full} (ms/step)	Memory (MB)
Pi-Beam MGN	14	35	12,512
Pi-Beam MGN-T	4.1	15	1,782
Deforming Plate MGN-T	2.3	3.2	1,752

Table 6: Computational cost of MGN and MGN-T.

MGN-T required approximately 4 hours on the Pi-beam dataset and 8 hours on the Deforming plate dataset, highlighting the computational efficiency of the proposed approach.

5 Discussion

Standard MeshGraphNet relies on deep stacked message-passing neural networks to propagate information across nodes in the mesh. This method has shown to be effective for coarse meshes; however, it becomes inefficient for high-resolution or industrial-scale meshes, as the number of iterations required grows rapidly with mesh size to prevent message passing under-reach. In contrast, MGN-T combines the geometric inductive bias of MeshGraphNet with the global processing capability of Transformers. By using a physics-attention Transformer, MGN-T updates all nodal states simultaneously, directly capturing long-range interactions and eliminating the need for deep message-passing stacks. This design addresses a fundamental bottleneck in MGN and allows for training on large, complex meshes without requiring graph reduction or hierarchy.

MGN-T operates directly on high-resolution meshes, naturally handling varying geometries, mesh topologies, numbers of nodes, and boundary conditions. This capability facilitates training on industrial-scale datasets for real-world engineering applications and enables the utilization of previously simulated data with minimal human intervention. In our experiments, MGN-T successfully simulates impact dynamics with self-contact under a plastic regime. We show its superiority over standard MGN, which fails. MGN-T captures complex physical behaviour, and its physical consistency is further evaluated for the plastic hardening and its relationships with the remaining physical state variables.

On the deforming plate dataset, MGN-T achieves competitive results compared to state-of-the-art approaches, demonstrating low error propagation in both single-step and full-rollout predictions. Compared to other approaches, MGN-T requires a fraction (roughly 1/4) of the parameters, making it a much lighter model, being its training and inference fast and efficient. These results confirm that the proposed method is a promising off-the-shelf approach for simulating solid mechanics phenomena, as it does not require any pre-processing, coarsening, or segmentation, unlike other hierarchical graph-based approaches.

5.1 Limitations and Future Work

MGN-T effectively overcomes the under-reaching bottleneck of standard MGN. Further exploration is needed for extremely large 3D simulations or problems involving different physics, such as fluid dynamics in Eulerian description, which are out of scope for this paper. Future work could investigate hybrid strategies that combine MGN-T with inductive biases of physical nature to further enhance accuracy and efficiency.

Acknowledgements

This work was supported by the Spanish Ministry of Science and Innovation, AEI/10.13039/501100011033, through Grant number PID2023-147373OB-I00, and by the Ministry for Digital Transformation and the Civil Service, through the ENIA 2022 Chairs for the creation of university-industry chairs in AI, through Grant TSI-100930-2023-1.

This material is also based upon work supported in part by the Army Research Laboratory and the Army Research Office under contract/grant number W911NF2210271.

The authors also acknowledge the support of ESI Group, Keysight Technologies, through the chair at the University of Zaragoza.

References

- [1] J. Brandstetter, D. Worrall, and M. Welling, “Message passing neural PDE solvers,” *arXiv:2202.03376*, 2022.

- [2] F. Pichi, B. Moya, and J. S. Hesthaven, “A graph convolutional autoencoder approach to model order reduction for parametrized PDEs,” *J. Comput. Phys.*, vol. 501, p. 112762, 2024.
- [3] M. Gorpinich *et al.*, “Bridging data and physics: A graph neural network-based hybrid twin framework,” *arXiv:2512.15767*, 2025.
- [4] D. Di Lorenzo *et al.*, “Physics-informed and graph neural networks for enhanced inverse analysis,” *Eng. Comput.*, vol. 42, no. 7, pp. 2427–2455, 2025.
- [5] M. Tomasetto *et al.*, “Reduced order modeling with shallow recurrent decoder networks,” *Nat. Commun.*, vol. 16, no. 1, p. 10260, 2025.
- [6] Q. Hernández *et al.*, “Structure-preserving neural networks,” *J. Comput. Phys.*, vol. 426, p. 109950, 2021.
- [7] Q. Hernández *et al.*, “Thermodynamics-informed graph neural networks,” *IEEE Trans. Artif. Intell.*, vol. 5, no. 3, pp. 967–976, 2022.
- [8] C. Bermejo *et al.*, “MeshGraphNets informed locally by thermodynamics for the simulation of flows around arbitrarily shaped objects,” *Adv. Model. Simul. Eng. Sci.*, vol. 12, no. 1, p. 27, 2025.
- [9] Q. Hernández *et al.*, “Port-metriplectic neural networks: Thermodynamics-informed machine learning of complex physical systems,” *Comput. Mech.*, vol. 72, no. 3, pp. 553–561, 2023.
- [10] A. Gruber, K. Lee, and N. Trask, “Reversible and irreversible bracket-based dynamics for deep graph neural networks,” in *Proc. Adv. Neural Inf. Process. Syst. (NeurIPS)*, vol. 36, pp. 38454–38484, 2023.
- [11] D. Roznowicz *et al.*, “Large-scale graph machine learning surrogate models for 3D flowfield prediction in external aerodynamics,” *Adv. Model. Simul. Eng. Sci.*, vol. 11, no. 1, p. 6, 2024.
- [12] N. R. Franco *et al.*, “Deep learning-based surrogate models for parametrized PDEs: Handling geometric variability through graph neural networks,” *Chaos*, vol. 33, no. 12, 2023.
- [13] A. Tierz *et al.*, “On the feasibility of foundational models for the simulation of physical phenomena,” *Int. J. Numer. Methods Eng.*, vol. 126, no. 6, p. e70027, 2025.
- [14] Z. Zhang, Y. Shin, and G. E. Karniadakis, “GFINNs: GENERIC formalism informed neural networks for deterministic and stochastic dynamical systems,” *Phil. Trans. R. Soc. A*, vol. 380, no. 2229, p. 20210207, 2022.
- [15] A. Tierz *et al.*, “Graph neural networks informed locally by thermodynamics,” *Eng. Appl. Artif. Intell.*, vol. 144, p. 110108, 2025.
- [16] A. Vaswani *et al.*, “Attention is all you need,” in *Proc. Adv. Neural Inf. Process. Syst. (NeurIPS)*, 2017.
- [17] A. Sanchez-Gonzalez *et al.*, “Learning to simulate complex physics with graph networks,” in *Proc. Int. Conf. Mach. Learn. (ICML)*, vol. 119, pp. 8459–8468, 2020.
- [18] T. Pfaff *et al.*, “MeshGraphNets: Learning the physics of complex systems,” in *Proc. Int. Conf. Learn. Represent. (ICLR)*, 2021.
- [19] Y.-Y. Youn, H. Li, and T. Pfaff, “HTCM: Transformer-based collision and diffusion modelling in learned simulators,” in *Proc. Int. Conf. Learn. Represent. (ICLR)*, 2024.
- [20] H. Li *et al.*, “A new graph-based surrogate model for rapid prediction of crashworthiness performance of vehicle panel components,” *arXiv:2503.17386*, 2025.
- [21] T. Würth *et al.*, “Diffusion-based hierarchical graph neural networks for simulating nonlinear solid mechanics,” in *Proc. Adv. Neural Inf. Process. Syst. (NeurIPS)*, 2025.
- [22] L. Tesán *et al.*, “On the under-reaching phenomenon in message passing neural PDE solvers: Revisiting the CFL condition,” *Comput. Methods Appl. Mech. Eng.*, vol. 449, p. 118476, 2026.
- [23] H. Zhou *et al.*, “A multi-level graph-based surrogate model for real-time high-fidelity sheet forming simulations,” *Adv. Eng. Informatics*, vol. 66, p. 103458, 2025.
- [24] J. C. Simo, “Numerical analysis and simulation of plasticity,” in *Handbook of Numerical Analysis*, vol. 6, pp. 183–499, 1998.
- [25] A. A. Jadoon, K. A. Meyer, and J. N. Fuhg, “Automated model discovery of finite strain elastoplasticity from uniaxial experiments,” *Comput. Methods Appl. Mech. Eng.*, vol. 435, p. 117653, 2025.
- [26] S. Rezaei, A. Moeineddin, and A. Harandi, “Learning solution of nonlinear constitutive material models using physics-informed neural networks: COMM-PINN,” *arXiv:2304.06044*, 2023.
- [27] M. Raissi, P. Perdikaris, and G. E. Karniadakis, “Physics-informed neural networks: A deep learning framework for solving forward and inverse problems involving nonlinear partial differential equations,” *J. Comput. Phys.*, vol. 378, pp. 686–707, 2019.

- [28] H. Luo *et al.*, “Transolver++: An accurate neural solver for PDEs on million-scale geometries,” *arXiv:2502.02414*, 2025.
- [29] H. Wu *et al.*, “Transolver: A fast transformer solver for PDEs on general geometries,” *arXiv:2402.02366*, 2024.
- [30] B. Alkin *et al.*, “AB-UPT: Scaling neural CFD surrogates for high-fidelity automotive aerodynamics simulations via anchored-branched universal physics transformers,” *arXiv:2502.09692*, 2024.
- [31] E. Jang, S. Gu, and B. Poole, “Categorical reparameterization with Gumbel–Softmax,” in *Proc. Int. Conf. Learn. Represent. (ICLR)*, 2017.
- [32] Y. Cao *et al.*, “Efficient learning of mesh-based physical simulation with bi-stride multi-scale graph neural network,” in *Proc. Int. Conf. Mach. Learn. (ICML)*, vol. 202, pp. 3541–3558, 2023.
- [33] M. Lino *et al.*, “Multi-scale rotation-equivariant graph neural networks for unsteady Eulerian fluid dynamics,” *Phys. Fluids*, vol. 34, p. 087110, 2022.
- [34] S. Janny *et al.*, “EAGLE: Large-scale learning of turbulent fluid dynamics with mesh transformers,” in *Proc. Int. Conf. Learn. Represent. (ICLR)*, 2023.
- [35] H. Deng *et al.*, “EvoMesh: Adaptive physical simulation with hierarchical graph evolutions,” in *Proc. Int. Conf. Mach. Learn. (ICML)*, vol. 267, pp. 13327–13346, 2025.
- [36] P. Garnier, J. Viquerat, and E. Hachem, “Multi-grid graph neural networks with self-attention for computational mechanics,” *Phys. Fluids*, vol. 37, no. 8, p. 087140, 2025.
- [37] B. Lei, V. Castillo, and Y. Hu, “M4GN: Mesh-based multi-segment hierarchical graph network for dynamic simulations,” *Trans. Mach. Learn. Res.*, 2025.